Correction for the influence of velocity lenses on nonhyperbolic moveout inversion for VTI media

Mamoru Takanashi[1,2] & Ilya Tsvankin[1]

[1] *Center for Wave Phenomena, Geophysics Department, Colorado School of Mines, Golden, Colorado 80401*
[2] *Japan Oil, Gas and Metals National Corporation, Chiba, Japan*

ABSTRACT

Nonhyperbolic moveout analysis plays an increasingly important role in velocity model building because it provides valuable information for anisotropic parameter estimation. However, lateral heterogeneity associated with stratigraphic lenses such as channels and reefs can significantly distort the moveout parameters, even when the structure is relatively simple.

Here, we discuss nonhyperbolic moveout inversion for 2D models that include a low-velocity isotropic lens embedded in a VTI (transversely isotropic with a vertical symmetry axis) medium. Synthetic tests demonstrate that a lens can cause substantial, laterally varying errors in the normal-moveout velocity ($V_{\rm nmo}$) and the anellipticity parameter η. The area influenced by the lens can be identified using the residual moveout after the nonhyperbolic moveout correction and the dependence of errors in $V_{\rm nmo}$ and η on spreadlength.

To remove lens-induced traveltime distortions from prestack data, we propose an algorithm that involves estimation of the incidence angle of the ray passing through the lens for each recorded trace. Using the velocity-independent layer-stripping method of Dewangan and Tsvankin, we compute the lens-induced traveltime shift from the zero-offset time distortion (i.e., from "pull-up" or "push-down" anomalies).

Synthetic tests demonstrate that this algorithm substantially reduces the errors in the effective and interval parameters $V_{\rm nmo}$ and η. The corrected traces and reconstructed "background" values of $V_{\rm nmo}$ and η are suitable for anisotropic time imaging and producing a high-quality stack.

Key words: P-waves, anisotropy, transverse isotropy, velocity analysis, lateral heterogeneity, velocity lenses, nonhyperbolic moveout inversion, traveltime shifts

1 INTRODUCTION

Kinematics of P-wave propagation in VTI (transversely isotropic with a vertical symmetry axis) media are governed by the vertical velocity V_0 and the Thomsen parameters ϵ and δ (Tsvankin & Thomsen, 1994). P-wave reflection traveltime in laterally homogeneous VTI media above a horizontal or dipping reflector depends only on the normal moveout velocity $V_{\rm nmo}$ and the anellipticity parameter η (Alkhalifah & Tsvankin, 1995; Tsvankin, 2005):

$$V_{\rm nmo} = V_0\sqrt{1+2\delta}\,, \tag{1}$$

$$\eta = \frac{\epsilon-\delta}{1+2\delta}\,. \tag{2}$$

The parameters $V_{\rm nmo}$ and η, which control all P-wave time-processing steps, can be obtained from nonhyperbolic moveout or dip-dependent NMO velocity. In particular, the nonhyperbolic moveout equation introduced by Alkhalifah & Tsvankin (1995) and its extension for layered media (Alkhalifah, 1997; Grechka & Tsvankin, 1998; Tsvankin, 2005) have been widely used for estimating $V_{\rm nmo}$ and η and building anisotropic velocity models.

Nonhyperbolic moveout analysis is performed under the assumption that the overburden is laterally homogeneous on the scale of spreadlength. However, even

gentle structures often contain small-thickness lenses (such as channels and carbonate reefs), whose width is smaller than the spreadlength (Armstrong et al., 2001; Fujimoto et al., 2007; Takanashi et al., 2008; Jenner, 2009; see Figure 1). For isotropic media, lateral heterogeneity of this type has been recognized as one of the sources of the difference between the moveout and true medium velocities (Al-Chalabi, 1979; Lynn & Claerbout, 1982; Toldi, 1989; Blias, 2009). Such lens-induced errors in $V_{\rm nmo}$ lead to misties between seismic and well data (Fujimoto *et al.*, 2007).

Although the moveout parameters (especially η) were shown to be sensitive to correlated traveltime errors (Grechka & Tsvankin, 1998), overburden heterogeneity is seldom taken into account in nonhyperbolic moveout inversion. Grechka (1998) shows analytically that a constant lateral velocity gradient does not distort the estimates of $V_{\rm nmo}$ and η, if anisotropy and lateral heterogeneity are weak. The second and fourth horizontal velocity derivatives, however, can cause errors in $V_{\rm nmo}$ and η. Still, Grechka's (1998) results are limited to a single horizontal layer and cannot be directly applied to models with thin lenses.

Recently, isotropic traveltime tomography has been used to estimate the velocity inside the lens and remove the lens-induced velocity errors (Fujimoto *et al.*, 2007; Fruehn *et al.*, 2008). These case studies show the importance of integrating seismic and geologic information and understanding the relationship between the overburden heterogeneity and velocity errors. In principle, laterally varying anisotropy parameters can be estimated from anisotropic reflection tomography (e.g. Woodward *et al.*, 2008). However, if the lens location is unknown, lens-induced traveltimes shifts can hinder accurate parameter estimation on the scale of spreadlength.

Here, we study the influence of velocity lenses on nonhyperbolic moveout inversion for 2D VTI models. To analyze lens-induced distortions of reflection data, we perform finite-difference modeling and apply moveout inversion using the Alkhalifah-Tsvankin (1995) nonhyperbolic equation. We show that even a relatively thin velocity lens may cause pronounced errors in the moveout parameters $V_{\rm nmo}$ and η and describe several criteria that can help identify range of common-midpoint (CMP) locations, for which reflected rays cross the lens. To remove lens-induced traveltime shifts, we propose a correction algorithm designed for gently dipping anisotropic layers. Synthetic tests demonstrate that this algorithm suppresses lens-related distortions on the stacked section and substantially reduces errors in the effective and interval parameters $V_{\rm nmo}$ and η.

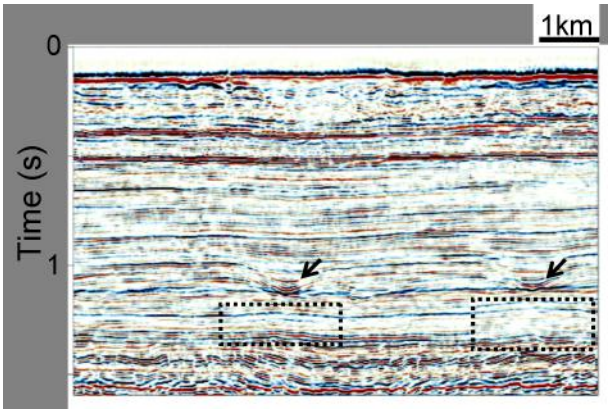

Figure 1. Time-migrated section from the central North Sea (after Armstrong *et al.*, 2001). Amplitude anomalies at the bottom of the channel-like structures (arrows) and pull-up anomalies below the structures (inside the rectangles) indicate the presence of lateral heterogeneity associated with the channel fills. Pull-up and push-down anomalies caused by high and low velocities, respectively, in channels or carbonate reefs are also observed in other hydrocarbon-producing regions, such as the Middle East and Northwest Australia.

2 DISTORTIONS CAUSED BY VELOCITY LENSES

To generate synthetic data, we perform finite-difference simulations (using Seismic Unix code *suea2df*; Juhlin, 1995) and ray tracing for 2D models that include a low-velocity isotropic lens inside a VTI layer. The parameters $V_{\rm nmo}$ and η are estimated from nonhyperbolic moveout inversion based on the Alkhalifah-Tsvankin (1995) equation:

$$t^2 = t_0^2 + \frac{x^2}{V_{\rm nmo}^2} - \frac{2\eta\, x^4}{V_{\rm nmo}^2[t_0^2\, V_{\rm nmo}^2 + (1+2\eta)x^2]}\,, \qquad (3)$$

where t is the P-wave traveltime as a function of the offset x and t_0 is the zero-offset time. Equation 3 can be applied to layered VTI media with the effective parameters given by (Tsvankin, 2005):

$$V_{\rm nmo}^2(N) = \frac{1}{t_0(N)} \sum_{i=1}^{N} (V_{\rm nmo}^{(i)})^2\, t_0^{(i)}, \qquad (4)$$

$$\eta(N) = \frac{1}{8}\left\{ \frac{1}{V_{\rm nmo}^4(N)\, t_0(N)} \left[\sum_{i=1}^{N} (V_{\rm nmo}^{(i)})^4 (1+8\eta^{(i)})\, t_0^{(i)} \right] - 1 \right\}, \qquad (5)$$

where $t_0^{(i)}$, $V_{\rm nmo}^{(i)}$, and $\eta^{(i)}$ are the interval values, and N is the number of layers.

Although the Alkhalifah-Tsvankin equation provides a good approximation for P-wave moveout in VTI media, the estimates of η are sensitive to correlated traveltime errors because of the tradeoff between η and $V_{\rm nmo}$

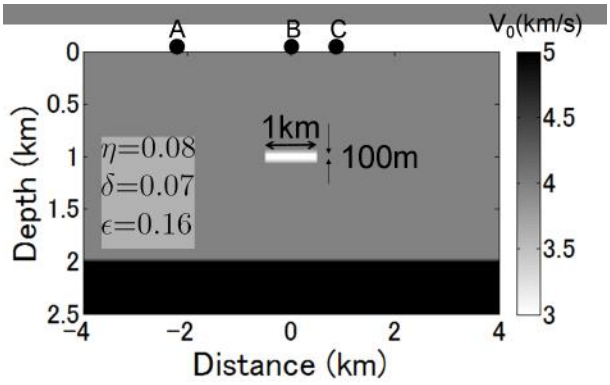

Figure 2. Single VTI layer with an isotropic lens. The lens velocity is 3 km/s; the background parameters are $V_0 = 4$ km/s, $\delta = 0.07$ and $\epsilon = 0.16$. Points A, B and C correspond to CMP locations discussed in the text. The test is performed for a spreadlength of 4 km; the target depth is 2 km.

(Grechka & Tsvankin, 1998). In our model, such errors are caused by an isotropic velocity lens in the overburden.

2.1 Single-layer model

First, we consider a rectangular lens embedded in a homogeneous VTI layer (Figure 2). The section in Figure 3 is computed by a finite-difference algorithm for common-midpoint (CMP) gathers outside the lens (location A) and at the center of the lens (location B). Whereas the lens does not distort traveltimes at location A, it causes a near-offset time delay of 17 ms and waveform distortions (related to the influence of the side and edges of the lens) in the mid-offset range at location B.

Using equation 3, we find the best-fit $V_{\rm nmo}$ and η for the target reflector from a 2D semblance scan; for comparison, we also perform conventional hyperbolic moveout inversion (Figure 4). The NMO velocity estimated from the nonhyperbolic equation at location A is close to the analytic value. At location B, however, $V_{\rm nmo}$ is about 10% greater, although the exact effective NMO velocity should decrease by 2% due to the low velocity inside the lens. At a CMP location near the edge of the lens (location C), $V_{\rm nmo}$ is 7% smaller than the exact value. Interestingly, nonhyperbolic moveout inversion produces an error in $V_{\rm nmo}$, which is two times larger than that obtained from hyperbolic moveout analysis.

The reason for the lens-induced distortion in $V_{\rm nmo}$ is described in Al-Chalabi (1979) and Biondi (2006) (Figures 5a,b). Near-offset rays at location B pass twice through the lens, while far-offset rays miss the lens completely. Since the lens has a lower velocity, this leads to a smaller traveltime difference between the near- and far-offset traces and, therefore, a higher NMO velocity. In contrast, for location C, the lens is missed by near-offset

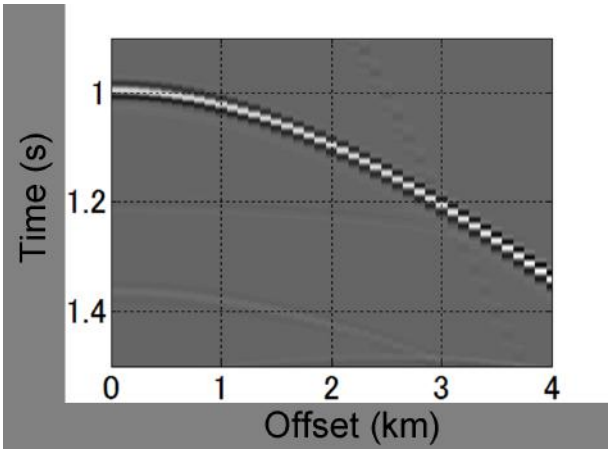

(a)

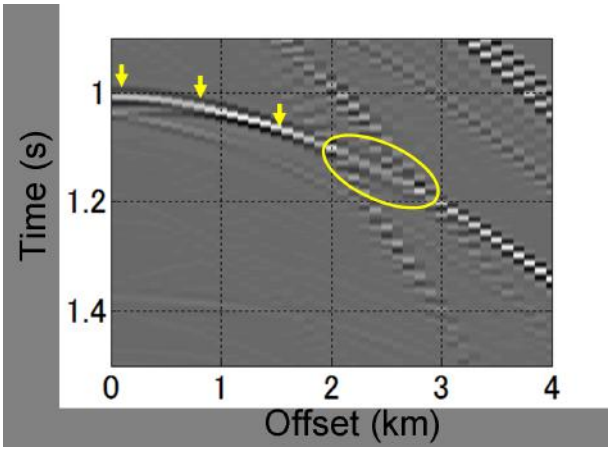

(b)

Figure 3. Comparison of CMP gathers for the model from Figure 2 computed (a) outside the lens (location A) and (b) above the center of the lens (location B) with a finite-difference algorithm. The traveltime shifts at near offsets (arrows) at location B cause significant errors in the parameters $V_{\rm nmo}$ and η. The lens-related waveform distortion at location B is contoured by the ellipse.

rays and the traveltime difference between the near and far offsets becomes larger, which reduces $V_{\rm nmo}$ (Figure 5b).

The nonhyperbolic inversion gives a closer approximation to the actual traveltime due to the contribution of the additional parameter η. Hence, the best-fit nonhyperbolic moveout curve at location B reproduces the increase in the near-offset traveltime, which causes a pronounced deviation of the estimated $V_{\rm nmo}$ from the exact value (Figure 5c). Note that the hyperbolic correction distorts the velocity $V_{\rm nmo}$ outside the lens due to the influence of nonhyperbolic moveout.

The laterally varying η-curve resembles the reversed version of the $V_{\rm nmo}$-curve. While in the absence

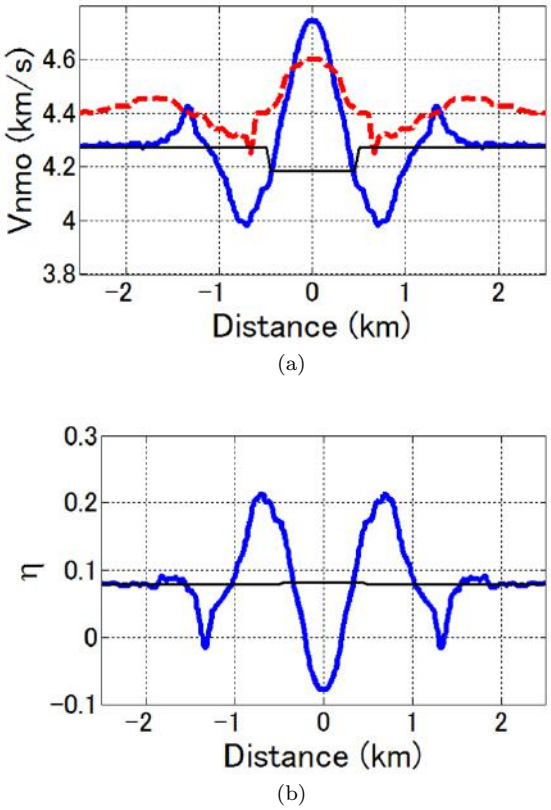

Figure 4. Lateral variation of the inverted (a) $V_{\rm nmo}$ and (b) η (bold solid lines) along the line using a spreadlength of 4 km (the spreadlength-to-depth ratio $X/D = 2$). The dashed line on plot (a) is the NMO velocity obtained from hyperbolic moveout analysis for the same spreadlength. The exact effective $V_{\rm nmo}$ (equation 4) and η (equation 5) are marked by thin solid lines.

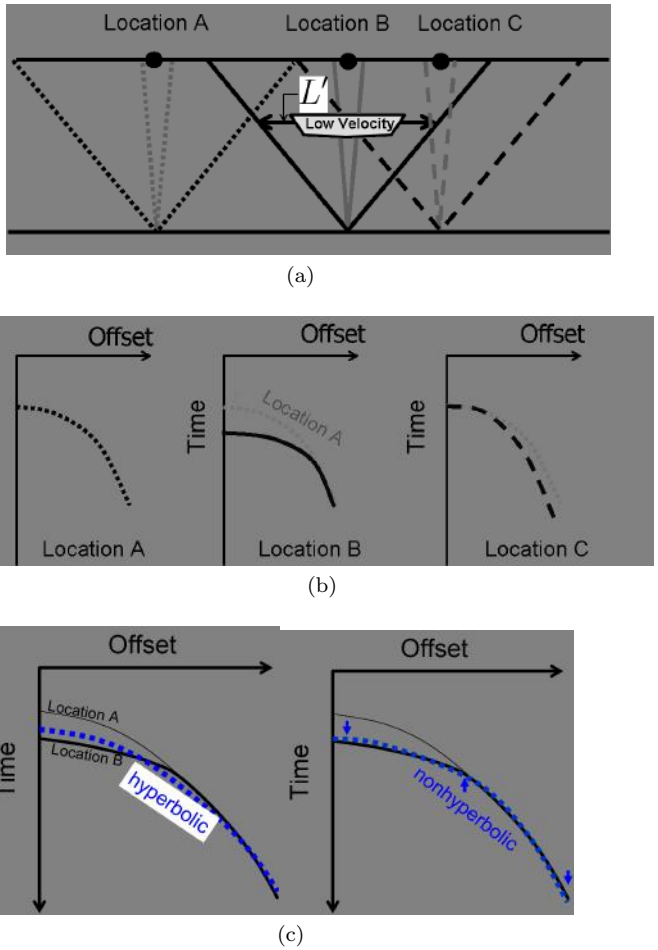

Figure 5. (a) Schematic picture of near- and far-offset raypaths from a horizontal reflector beneath a low-velocity lens at three CMP locations (modified from Biondi, 2006). (b) The influence of the lens on the moveout curves. The raypaths and moveout curves at locations A, B and C are shown by dotted, solid and dashed lines, respectively. (c) Schematic estimated moveout curves (dotted lines) obtained from hyperbolic (left) and nonhyperbolic (right) inversion at location B. The actual moveouts at locations A and B are shown by thin and bold solid lines, respectively.

of the lens the effective η at location B should almost coincide with the background $\eta = 0.08$, the estimated $\eta = -0.07$ is much smaller. The understated value of η is explained by the need to compensate for the overstated estimate of $V_{\rm nmo}$ in reproducing traveltimes at moderate and large offsets (Grechka & Tsvankin, 1998; Tsvankin, 2005). The magnitude of the variation (the difference between the largest and smallest values) in η along the line is close to 0.3.

2.2 Dependence of distortions on the lens parameters

Using ray-traced synthetic data, we investigate the dependence of the inverted moveout parameters on the velocity, width, and depth of the lens. The replacement of finite differences with ray tracing does not significantly change the inversion results.

As expected, the magnitude of the errors in $V_{\rm nmo}$ and η is proportional to the velocity contrast between the lens and the background (Figure 6a). When the spreadlength is fixed, the time distortions depend on the ratio W/L', where W is the width of the lens and L' is the maximum horizontal distance between the incident and reflected rays at the lens depth (Figure 5a). Note that L' decreases with increasing lens depth. For the model used in the test, the distortions in $V_{\rm nmo}$ and η are largest when the width of the lens is 0.5 km (or $W/L' = 0.25$) (Figure 6b). On the other hand, the error in $V_{\rm nmo}$ estimated from hyperbolic moveout inversion has a flat maximum for the width ranging from 0.5 km to 1.5 km.

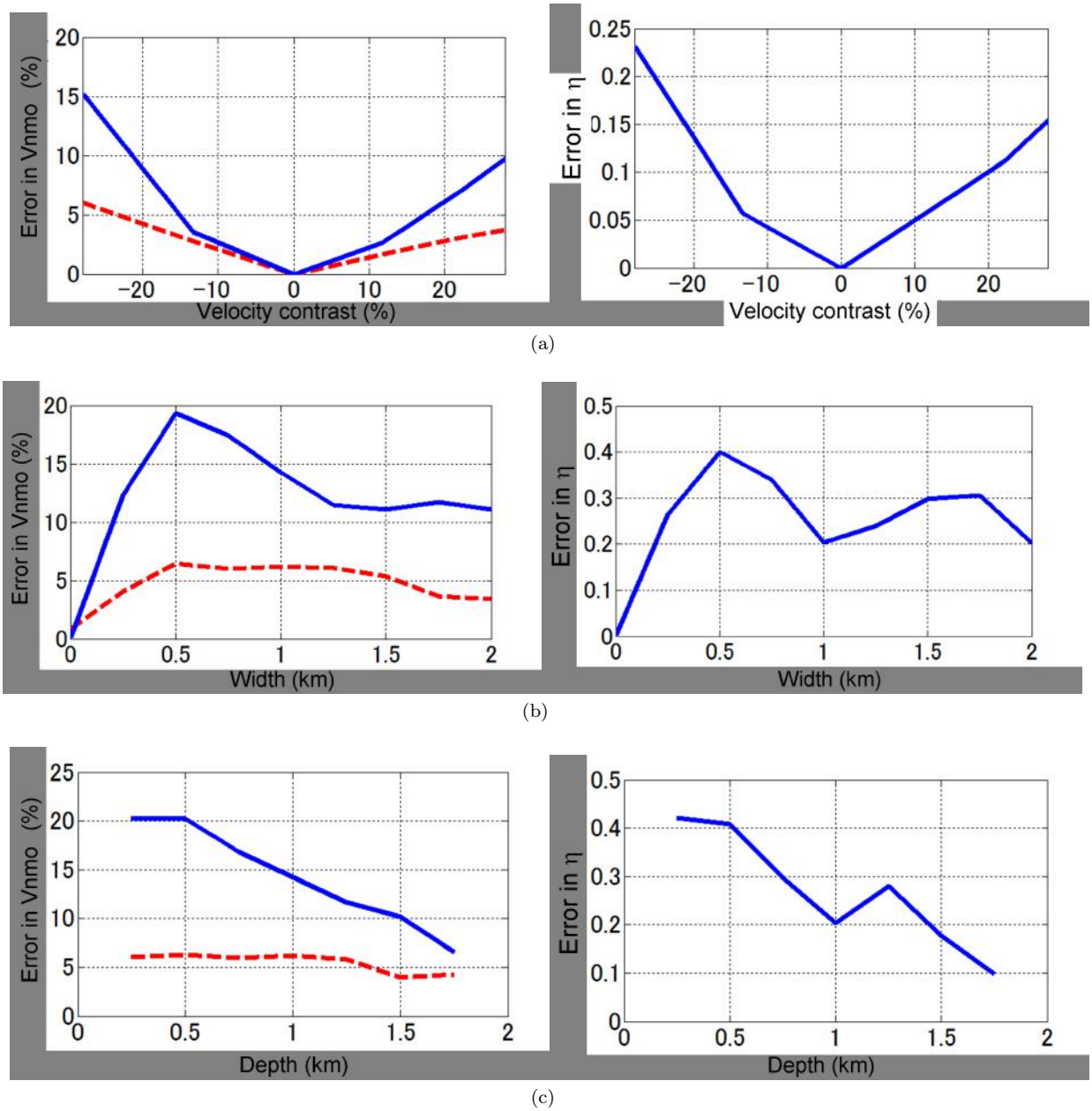

Figure 6. Dependence of the magnitude of the variation in V_{nmo} (left) and η (right) on (a) the velocity contrast defined as $(V_{\mathrm{lens}} - V_{\mathrm{back}})/V_{\mathrm{back}}$, where V_{lens} is the lens velocity and V_{back} is the background velocity, (b) the width and (c) the depth of the lens. V_{nmo} is obtained from nonhyperbolic (solid lines) and hyperbolic (dashed lines) moveout inversion. The spreadlength is 4 km (offset-to-depth ratio $X/D = 2$).

Since W/L' at the surface is 0.25 ($W = 1$ km, spreadlength is 4 km) in this model, a shallower lens causes larger errors in V_{nmo} and η (Figure 6c). For a depth of 0.25 km ($W/L' = 0.29$), the errors are close to the largest distortions for the test in Figure 6b.

2.3 Identifying lens-induced distortions

Identifying the range of CMP locations influenced by the lens is critical for avoiding the use of distorted parameters. It is clear from the above results that large variations of V_{nmo} and η on the scale of spreadlength are strong indications of the lens. Using the single-layer lens model, we suggest two additional indicators of the

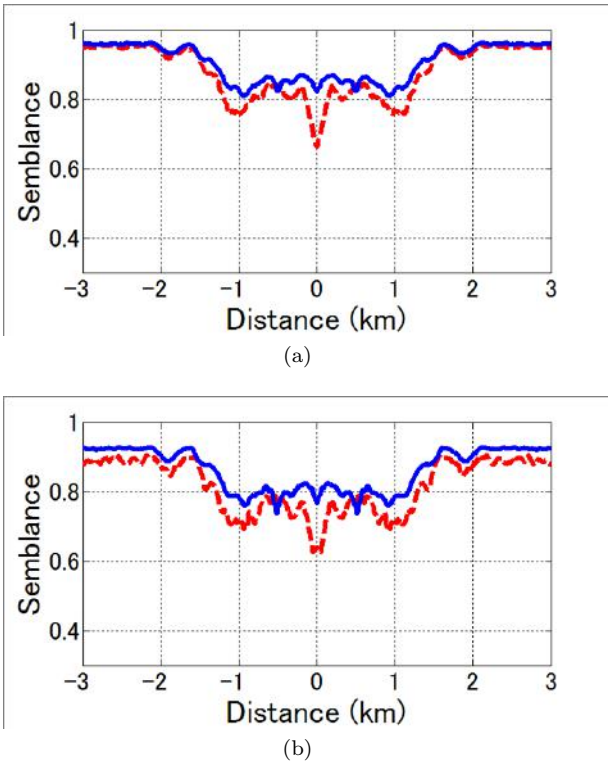

Figure 7. Semblance value for moveout-corrected gathers before (dashed line) and after (solid line) applying trim statics. The data were contaminated by random noise with the signal-to-noise ratio equal to (a) 10 and (b) 5.

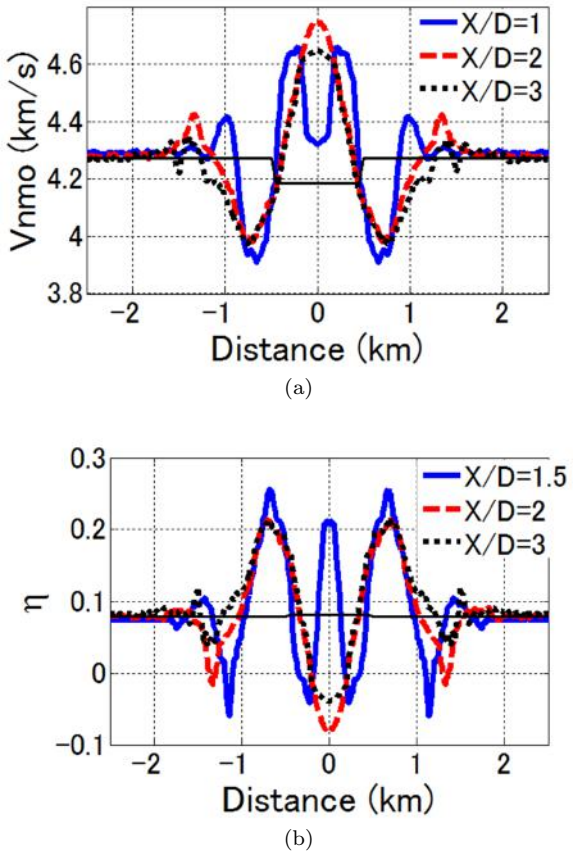

Figure 8. Dependence of (a) V_{nmo} and (b) η on the spreadlength-to-depth ratio (X/D).

lens – residual moveout after application of nonhyperbolic moveout correction and the dependence of V_{nmo} and η on spreadlength.

The moveout curve distorted by the lens cannot be completely flattened by the nonhyperbolic moveout equation. To estimate the magnitude of the residual moveout, one can use so-called trim statics (Ursenbach & Bancroft, 2001). Trim statics involves cross-correlation between a near-offset trace and all offset traces, which helps evaluate the statics shifts needed to eliminate the residual moveout. Due to the presence of residual moveout in the area influenced by the lens, application of trim statics increases the semblance (Figure 7). Still, the semblance value after trim statics at location B is lower than that at location A because of the lens-induced waveform distortions.

Trim statics, however, may not perform well when the data contain random or coherent noise (Ursenbach & Bancroft, 2001). If the signal-to-noise (S/N) ratio is less than five, trim statics increases the semblance by aligning noise components in the statics-corrected gather (Figure 7). Thus, trim statics can be used to delineate the area influenced by the lens only for relatively high S/N ratios.

Another possible lens indicator is the variation of the moveout parameters with spreadlength. As shown in Figure 8, the shape of the V_{nmo}- and η- curves is highly sensitive to the spreadlength-to-depth ratio (X/D). In contrast, the estimated moveout parameters at location A outside the lens are weakly dependent on spreadlength.

2.4 Layered model

The conclusions drawn above remain valid for a more realistic, layered model containing a parabola-shaped lens, which causes a maximum time distortion (or push-down anomaly) of 18 ms (Figure 9). We generate synthetic data with finite-differences and apply nonhyperbolic moveout inversion for the two interfaces (A and B) below the lens (Figure 10).

For a spreadlength of 4 km, the maximum distortion (the maximum deviation from the exact value) in V_{nmo} reaches approximately 9% for interface A and 11% for interface B (Figure 10), while the distortion in η

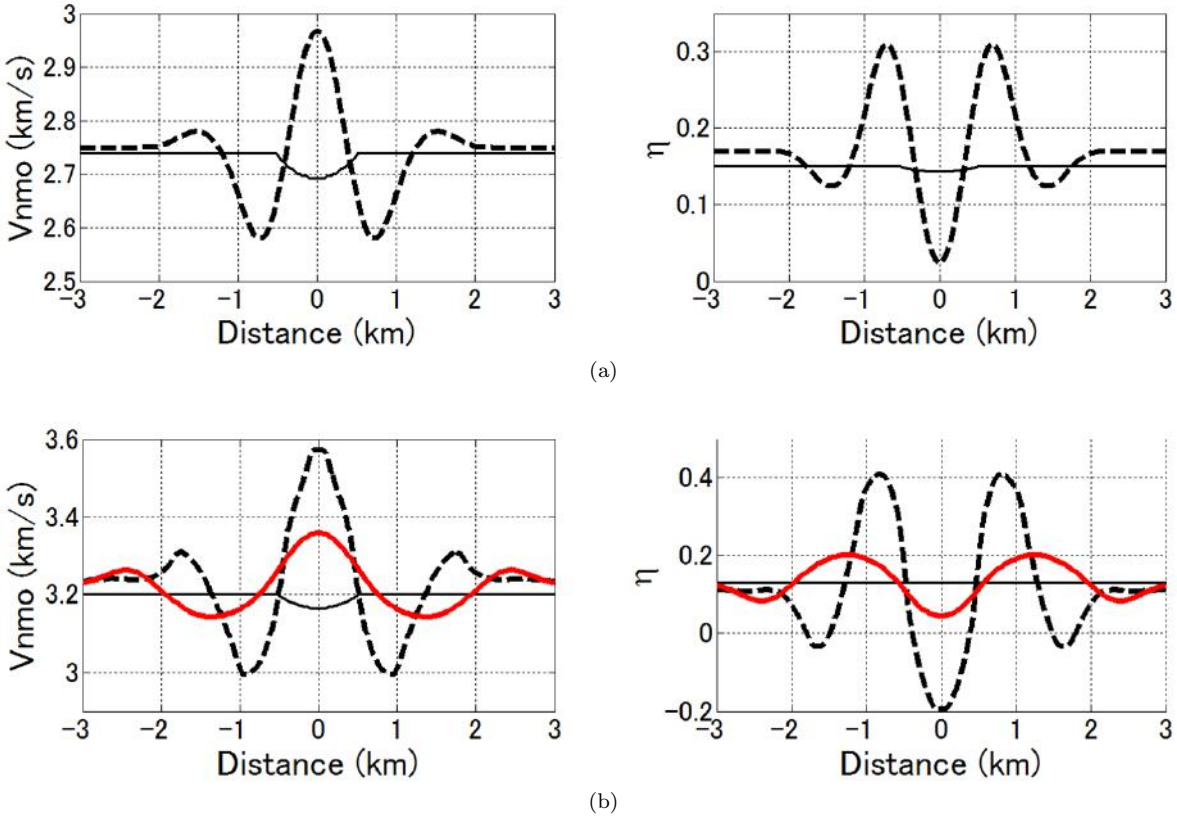

Figure 10. Lateral variation of estimated $V_{\rm nmo}$ (left) and η (right) for the model from Figure 9 for (a) interface A and (b) interface B. The dashed lines correspond to a spreadlength of 4 km, solid lines [only on plot (b)] to a spreadlength 6 km. The thin solid lines mark the exact parameters.

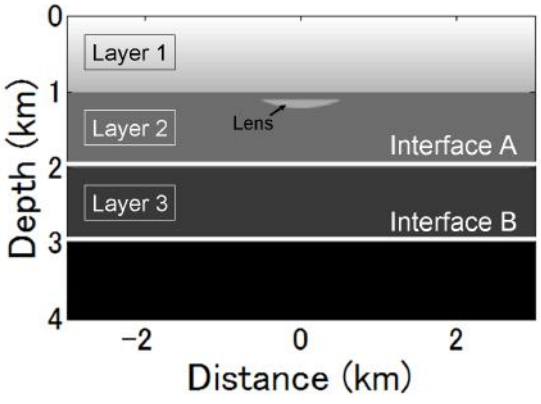

Figure 9. Layered model with a parabola-shaped lens. The first layer is isotropic and vertically heterogeneous; V_0 changes from 1.5 km/s at the surface to 2.5 km/s at the 1 km depth. The second layer is homogeneous VTI with $V_0 = 3.5$ km/s, $\delta = 0.07$ and $\epsilon = 0.16$ and contains an isotropic lens with $V_0 = 2.7$ km/s. The maximum thickness of the lens is 100 m. The third layer is homogeneous VTI with $V_0 = 4.2$ km/s, $\delta = 0.05$ and $\epsilon = 0.1$.

reaches 0.15 and 0.33, respectively. The larger errors for interface B are related to its lower ratio X/D.

When we use a spreadlength of 6 km ($X/D = 2$), the distortions in $V_{\rm nmo}$ and η for interface B decrease to 5% and 0.08, respectively. As is the case for a homogeneous background medium, the moveout-corrected gather exhibits residual moveout in the area influenced by the lens (Figure 11). Thus, the presence of residual moveout and the dependence of the moveout parameters on the spreadlength can serve as lens indicators for layered media as well.

3 CORRECTION ALGORITHM

It is clear from the modeling results that even a thin lens can cause significant errors in the parameters $V_{\rm nmo}$ and η. Another serious lens-induced distortion is the push-down anomaly on the stacked time section (Figure 12a). Although the time anomaly becomes smaller if the stack is produced using the background moveout parameters estimated away from the lens, the stacked event then has a smaller power because of a larger residual moveout

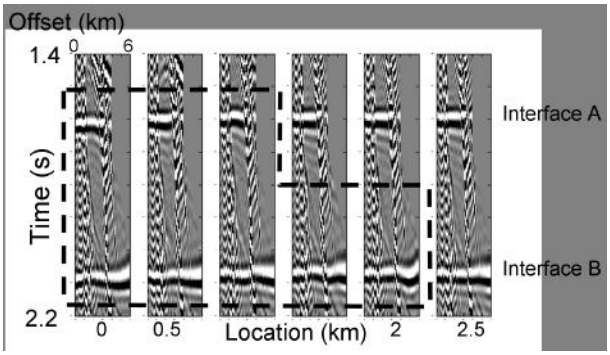

Figure 11. Moveout-corrected gathers computed using the best-fit parameters $V_{\rm nmo}$ and η. Residual moveout is observed inside the area marked by the dashed line.

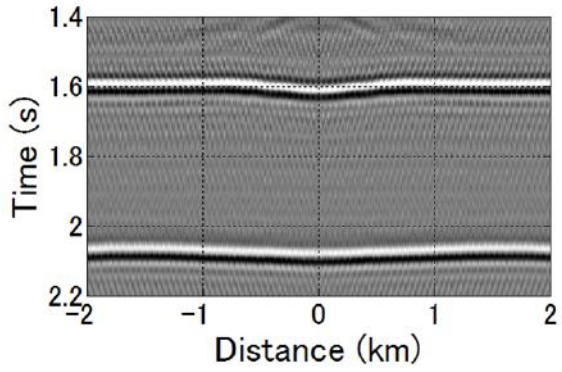

(a)

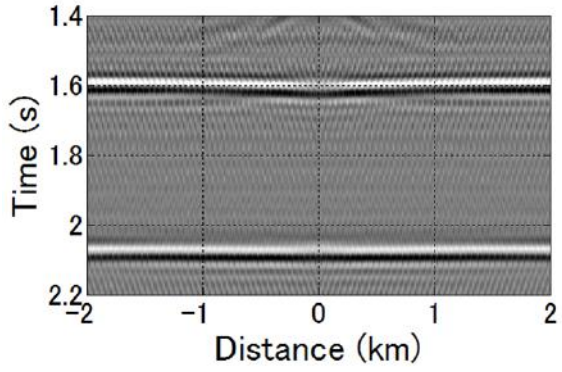

(b)

Figure 12. Stacked section generated using (a) the best-fit moveout parameters and (b) the background parameters.

(Figure 12b). Clearly, it is desirable to produce an accurate stacked section without reducing the stack power. Here, we introduce two methods for correcting P-wave data from layered VTI media for the influence of the lens. One of them is designed to mitigate the distortions on the stacked section using trim statics. The other method makes it possible to remove the traveltime distortions from each recorded trace and, therefore, obtain both accurate moveout parameters and a high-quality stack.

3.1 Trim statics

By eliminating residual moveout, trim statics makes all traces kinematically equivalent to the zero-offset trace (Figure 13a). Thus, trim statics increases stack power and generates a stack that kinematically reproduces the zero-offset section (compare Figure 13b with Figure 12a).

To remove the zero-offset time distortion, we assume that the zero-offset raypath is not influenced by the lens and remains vertical for all horizontal interfaces. Then the distortion of t_0 should be the same at interfaces A and B. This assumption allows us to use the estimated push-down at interface A for correcting the time distortions for both interfaces. The resulting stacked section is kinematically correct and has a high stack power (Figure 13c). However, as discussed above, trim statics works only for high S/N ratios and cannot be used to estimate the background values of $V_{\rm nmo}$ and η.

3.2 Prestack traveltime shifts

3.2.1 Method

The correction algorithm discussed here is designed for a horizontally layered overburden containing the lens, but the target reflector can be dipping or curved. Unlike the statics correction, this technique involves computation of traveltime shifts as functions of offset and target depth (Figure 14a). As the input data we use the zero-offset time shifts ("pull-up" or "push-down" anomalies, Δt_0) for the horizontal reflector immediately below the lens. The lens-related perturbation of the raypath is assumed to be negligible, so that the ray in the layer containing the lens can be considered straight. Then the ray crossing the lens can be reconstructed using the velocity-independent layer-stripping method (VILS) of Dewangan & Tsvankin (2006).

VILS builds the interval traveltime-offset function by performing kinematic downward continuation of the wavefield without knowledge of the velocity model. Each layer in the overburden is supposed to be laterally homogeneous with a horizontal symmetry plane, so that the raypath of any reflection event is symmetric with respect to the reflection point. The bottom of the target layer, however, can be curved and the layer itself can be heterogeneous. Wang & Tsvankin (2009) show that VILS provides more robust estimates of the interval moveout parameters in VTI and orthorhombic models than Dix-type equations.

VILS can be applied to our model under the as-

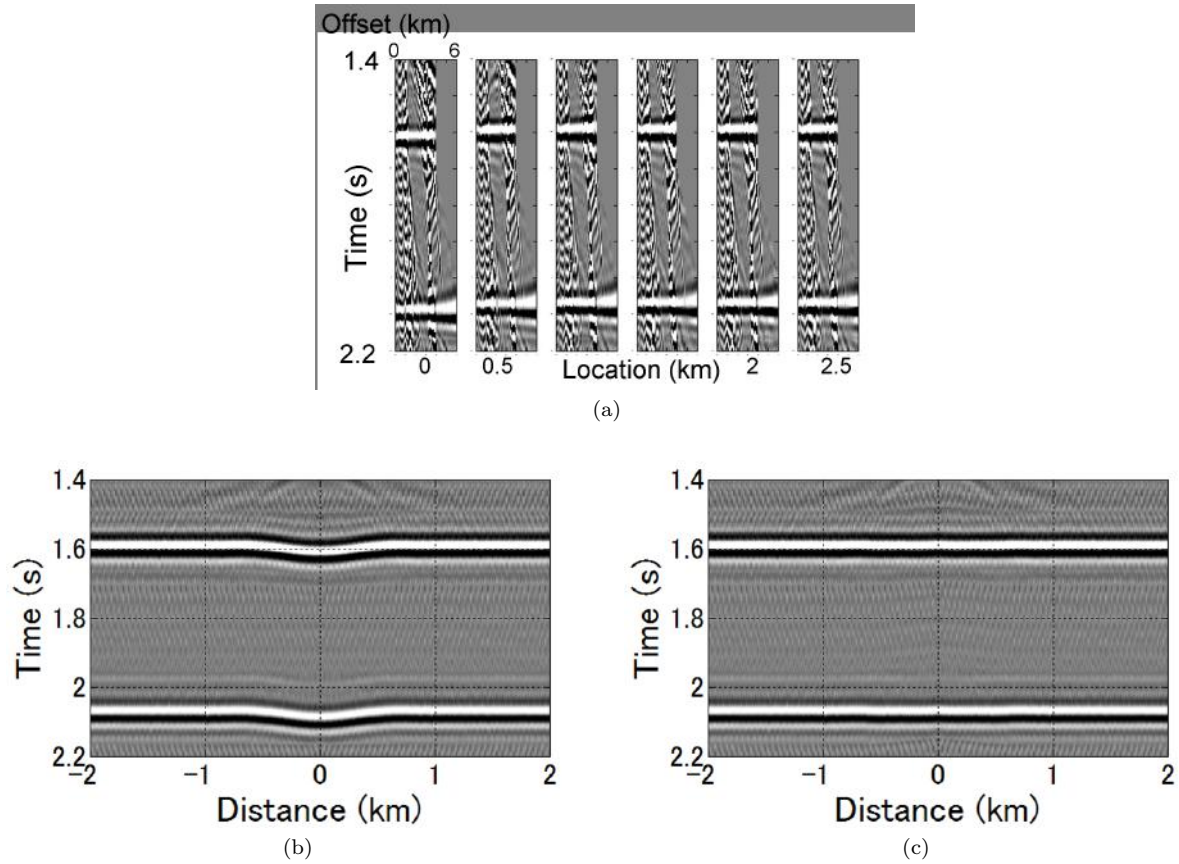

Figure 13. (a) Moveout-corrected gather after application of trim statics; (b) the stacked section after trim statics, and (c) the stacked section from plot (b) after removing the push-down anomaly at interface A.

sumption that the raypath in the overburden is not distorted by the lens. The idea of VILS is to identify reflections from the top and bottom of a certain layer that share the same upgoing and downgoing ray segments. This is accomplished by matching time slopes on common-receiver and common-source gathers. Application of VILS to the reflections from the target and top of the layer containing the lens yields the horizontal coordinates x_{T1} and x_{R1} (Figure 14a). Likewise, the coordinates x_{R2} and x_{T2} are estimated by combining the target event with the reflection from the bottom of the layer containing the lens.

Under the straight-ray assumption, we find the horizontal coordinates of the crossing points and the ray angles (Figures 14a,b):

$$x_{TL} = x_{T1} + \frac{z'_{TL}(x_{T2} - x_{T1})}{z}, \tag{6}$$

$$x_{RL} = x_{R1} - \frac{z'_{RL}(x_{R1} - x_{R2})}{z}, \tag{7}$$

$$\cos\theta_{TL} = \frac{z}{\sqrt{(x_{T2} - x_{T1})^2 + z^2}}, \tag{8}$$

$$\cos\theta_{RL} = \frac{z}{\sqrt{(x_{R1} - x_{R2})^2 + z^2}}, \tag{9}$$

where z is the thickness of the layer with the lens, and z'_{TL} and z'_{RL} are the distances from the lens to the top of the layer at locations x_{TL} and x_{RL}, respectively.

If the lens produces a sufficiently strong reflection and the layer is vertically homogeneous, the ratio z'/z can be estimated from the corresponding zero-offset traveltimes (t'/t). In the layered model, we can clearly identify the lens reflection at t = 1.15 s on the stacked section (Figure 15a). This indicates that the horizontal coordinates and the ray angles can be estimated without complete information about the velocity and anisotropy parameters. Then the total lens-related traveltime shift for the target event $(\Delta t_{\rm ta})$ can be computed as

$$\Delta t_{\rm ta} = \frac{1}{2}\left(\frac{\Delta t_0\,(x_{TL}, 0)}{\cos\theta_{TL}} + \frac{\Delta t_0\,(x_{RL}, 0)}{\cos\theta_{RL}}\right), \tag{10}$$

where $\Delta t_0(x_{TL}, 0)$ and $\Delta t_0(x_{RL}, 0)$ are the zero-offset time distortions below the lens at locations x_{TL} and

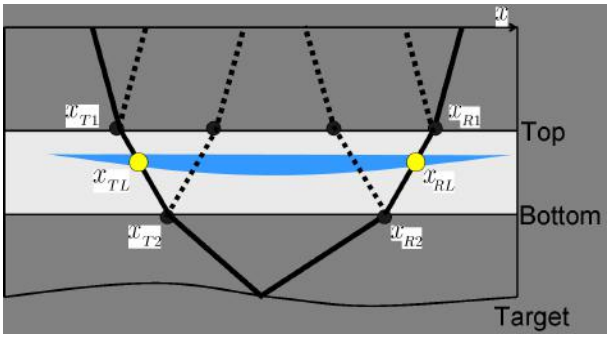

(a)

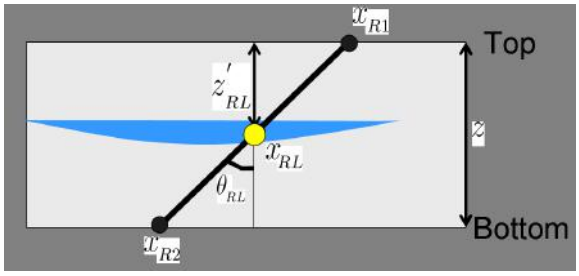

(b)

Figure 14. (a) Ray diagram of the correction algorithm. The horizontal coordinates x_{T1}, x_{T2} and x_{R1}, x_{R2} are determined from the velocity-independent layer-stripping method. (b) Upgoing ray segment crossing the lens. Using the values of z'_{RL} and z, we can compute the horizontal location of the crossing point (x_{RL}) and the ray angle (θ_{RL}).

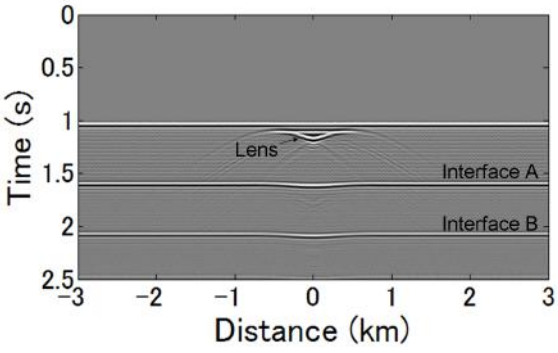

(a)

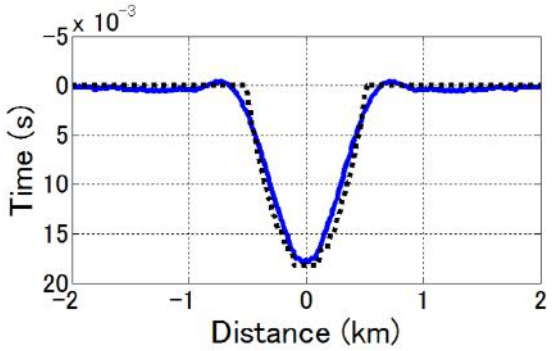

(b)

Figure 15. (a) Near-offset stacked section obtained for the offset range from 0 to 200 m, and (b) the magnitude of the push-down anomaly (solid line) estimated by picking the maximum amplitude along interface A. The dotted line in (b) is the exact Δt_0.

x_{RL}, respectively. Both $\Delta t_0(x_{TL}, 0)$ and $\Delta t_0(x_{RL}, 0)$ can be estimated from the near-offset stack. The ray angles θ_{TL} and θ_{RL} do not have to be the same, which makes the algorithm suitable for dipping or curved target reflectors.

After the correction, the kinematics of the prestack data should be close to the reflection traveltime described by the background values of $V_{\rm nmo}$ and η. The interval parameters $V_{\rm nmo}^{(i)}$ and $\eta^{(i)}$ can be computed using the layer-stripped data corrected for the lens-induced time shifts. The removal of the time distortions also helps generate an accurate stacked section.

3.2.2 Synthetic test

The prestack correction algorithm is tested here on the layered model from Figure 9. First, we need to estimate the three required input quantities: Δt_0, the ratio z'/z, and the thickness z of the layer containing the lens. The values of Δt_0 (Figure 15b) and z'/z (t'/t) are obtained from the near-offset stacked section (Figure 15a). For purposes of this test, the thickness of the layer containing the lens is assumed to be known.

Application of traveltime shifts computed from equation 10 eliminates the time-varying push-down anomaly and increased the S/N ratio of the stacked section (Figure 16a). Also, the correction significantly reduces the residual moveout in the moveout-corrected gathers (Figure 16b) and the errors in the effective parameters $V_{\rm nmo}$ and η (Figure 17a). For interface B, the distortion in $V_{\rm nmo}$ decreases from 5% to less than 1%, and in η from 0.08 to 0.02. Figure 17b shows that the correction algorithm also produces much more accurate interval parameters $V_{\rm nmo}$ and η estimated from the layer-stripped data. The remaining errors are largely caused by the straight-ray assumption for the layer containing the lens.

It is important to evaluate the sensitivity of the parameter estimation to errors in the input data. Extensive testing shows that when the error in Δt_0 is smaller than 25%, the moveout-corrected gather is almost flat. To test the sensitivity to the ratio z'/z, we move the lens down by 100 m and 200 m, which corresponds to 10% and 20% errors in z'/z. Although distortions in the moveout-corrected gather become noticeable when the error reaches 20%, the magnitude of the residual moveout is still much smaller than that before the correction.

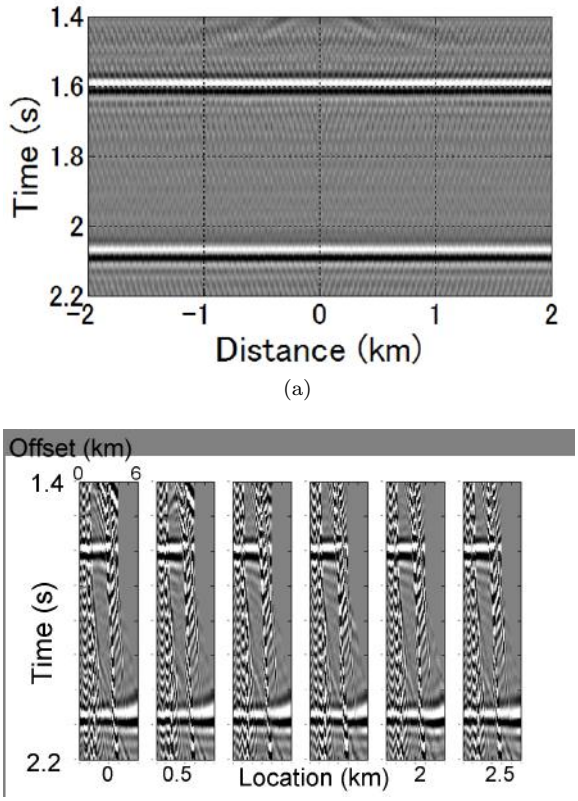

Figure 16. (a) Stacked section and (b) moveout-corrected gathers obtained after applying prestack traveltime shifts that compensate for the influence of the lens.

Finally, a thickness error up to 20% proves to have little impact on the output of the correction algorithm. An accurate stacked section can be generated even for somewhat larger errors in these input quantities.

4 DISCUSSION

The correction algorithm requires knowledge of the zero-offset time anomaly Δt_0, the ratio z'/z and the thickness z of the lens-containing layer. In the synthetic test, Δt_0 was accurately estimated from the push-down anomaly on the near-offset stacked section, and the ratio z'/z was obtained from the corresponding time ratio t'/t using the reflection from the lens (Figure 15). Since depth uncertainty seldom exceeds 20% in practice, errors in z are not expected to have a significant impact on the correction results.

The suggested approach should be applicable to many field data sets. For example, the time section from the central North Sea in Figure 1 contains channel-like structures and pull-up anomalies (marked area in Figure 1), which indicate the presence of high-velocity channel fills (Armstrong *et al.*, 2001). The lens reflections are sufficiently strong for estimating the ratio t'/t (and, therefore, z'/z), and the pull-up time anomaly can be accurately measured as well.

Our algorithm can also be applied to layered media with multiple lenses, if it is possible to estimate the values of Δt_0 and z'/z for each lens separately. Then the total traveltime shifts are obtained by summing the individual lens-induced time distortions. However, the algorithm will produce distorted time shifts when a layer contains multiple lenses or the lens reflections cannot be identified. Also, the algorithm assumes a laterally homogeneous overburden and straight rays in the layers containing the lenses. Therefore, the correction may become inaccurate when the overburden includes dipping interfaces or has a strong velocity contrast between the lens and the background.

5 CONCLUSIONS

We demonstrated that a relatively thin velocity lens may cause significant, laterally varying distortions in the moveout parameters $V_{\rm nmo}$ and η estimated from nonhyperbolic moveout analysis. The magnitude of the distortion depends on the width and depth of the lens and is proportional to the velocity contrast between the lens and the background. The error in $V_{\rm nmo}$ is larger after nonhyperbolic moveout inversion compared with the conventional hyperbolic algorithm applied for the same spreadlength, particularly when the lens is narrow or is located in a shallow layer. Hence, although nonhyperbolic moveout analysis produces smaller residual moveout and higher stacking power than the hyperbolic equation, it does not guarantee a more accurate estimation of NMO velocity in the presence of lateral heterogeneity.

Identifying the area influenced by the lens is critical for avoiding use of distorted moveout parameters. We showed that the residual moveout can serve as a lens indicator because the lens-induced distortion cannot be completely removed by nonhyperbolic moveout inversion. The presence of residual moveout can be identified from the increase in semblance after application of trim statics, provided the signal-to-noise ratio is sufficiently high. A lens also manifests itself by making the moveout parameters strongly dependent on spreadlength and the lateral coordinate.

To correct for lens-induced traveltime shifts on prestack data, we developed an algorithm based on velocity-independent layer stripping (VILS). Synthetic tests confirmed that the algorithm successfully removes lens-induced distortions on the stacked section and substantially reduces the errors in the effective and interval parameters $V_{\rm nmo}$ and η. The correction requires estimates of the zero-offset time distortion Δt_0, the thickness z of the layer containing the lens and the ratio z'/z, where z' is the distance between the lens and the top of

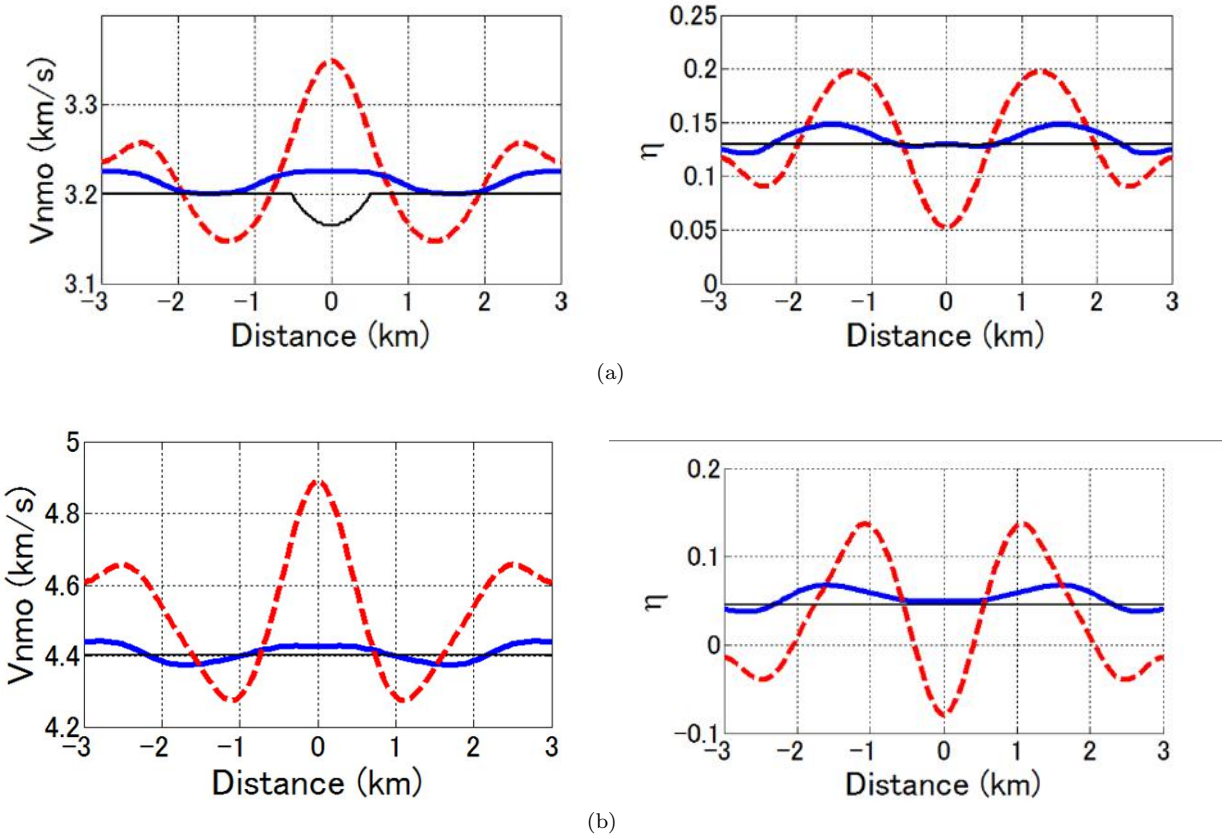

Figure 17. (a) Inverted effective parameters $V_{\rm nmo}$ (left) and η (right) for interface B before (dashed line) and after (thick solid line) applying the correction algorithm ($X/D = 2$). (b) The interval parameters $V_{\rm nmo}$ and η in the third layer (2-3 km) estimated before (dashed line) and after (thick solid line) applying the correction algorithm. The spreadlength (before applying VILS) is 6 km. Thin solid lines mark the exact parameters.

the lens-containing layer. The parameters Δt_0 and z'/z can be obtained from reflection data, while z cannot be found without additional (e.g., borehole) information. However, errors up to 20% in the Δt_0 and z, as well as a 10% error in the ratio z'/z, do not significantly hamper the performance of the algorithm.

Although we presented the correction method for a 2D model that contains a single lens, it can be extended to wide-azimuth data from layered media with well-separated multiple lenses. Potentially, the 3D version of the algorithm can be used to correct for the influence of small-scale lateral heterogeneities on azimuthal moveout inversion.

6 ACKNOWLEDGMENTS

We are grateful to members of the A(nisotropy)-Team of the Center for Wave Phenomena (CWP), Colorado School of Mines (CSM), for helpful discussions. This work was supported by Japan Oil, Gas and Metals National Corporation (JOGMEC) and the Consortium Project on Seismic Inverse Methods for Complex Structures at CWP.

REFERENCES

Al-Chalabi, 1979, Velocity determination from seismic reflection data , Applied Science Publishers.

Alkhalifah, T., and Tsvankin, I., 1995, Velocity analysis for transversely isotropic media: Geophysics, **60**, 1550–1566.

Alkhalifah, T., 1997, Velocity analysis using nonhyperbolic moveout in transversely isotropic media: Geophysics, **62**, 1839–1854.

Armstrong, T., McAteer, J., and Connolly, P., 2001, Removal of overburden velocity anomaly effects for depth conversion: Geophysical Prospecting, **49**, 79–99.

Biondi, B. L., 2006, 3D seismic imaging , Society of Exploration Geophysicists.

Blias, E., 2009, Stacking velocities in the presence of

overburden velocity anomalies: Geophysical Prospecting, **57**, 323–341.

Dewangan, P., and Tsvankin, I., 2006, Velocity-independent layer stripping of PP and PS reflection traveltimes: Geophysics, **71**, no. 4, U59–U65.

Fruehn, J., Jones, I. F., Valler, V., Sangvai, P., Biswal, A., and Mathur, M., 2008, Resolving near-seabed velocity anomalies: Deep water offshore eastern India: Geophysics, **73**, no. 5, VE235–VE241.

Fujimoto, M., Takanashi, M., Szczepaniak, M., and Yoshida, T., 2007, Application of prestack depth migration across the Ichthys field, Browse basin: ASEG Annual Meeting, Expanded Abstracts.

Grechka, V., and Tsvankin, I., 1998, Feasibility of nonhyperbolic moveout inversion in transversely isotropic media: Geophysics, **63**, 957–969.

Grechka, V., 1998, Transverse isotropy versus lateral heterogeneity in the inversion of P-wave reflection traveltimes: Geophysics, **63**, 204–212.

Jenner, E., 2009, Data example and modelling study of P-wave azimuthal anisotropy potentially caused by isotropic velocity heterogeneity: First Break, **27**, 45–50.

Juhlin, C., 1995, Finite-difference elastic wave propagation in 2D heterogeneous transversely isotropic media: Geophysical Prospecting, **43**, 843–858.

Lynn, W. S., and Claerbout, J. F., 1982, Velocity estimation in laterally varying media: Geophysics, **47**, 884–897.

Takanashi, M., Kaneko, M., Monzawa, N., Imahori, S., Ishibashi, T., and Sakai, A., 2008, Removal of overburden channel effects through channel velocity modeling and prestack depth migration for an oil field offshore Abu-Dhabi: Abu Dhabi International Petroleum Exhibition and Conference, SPE 117982.

Toldi, J., 1989, Velocity analysis without picking: Geophysics, **54**, 191–199.

Tsvankin, I., and Thomsen, L., 1994, Nonhyperbolic reflection moveout in anisotropic media: Geophysics, **59**, 1290–1304.

Tsvankin, I., 2005, Seismic signatures and analysis of reflection data in anisotropic media , 2nd ed, Elsevier Science Publishing Company, Inc.

Ursenbach, C. P., and Bancroft, J. C., 2001, Playing with fire: Noise alignment in trim and residual statics: 71th Annual Internatinal Meeting, SEG, Expanded Abstracts, 1973-1976.

Wang, X., and Tsvankin, I., 2009, Estimation of interval anisotropy parameters using velocity-independent layer stripping: Geophysics, **74**, no. 5, WB117–WB127.

Woodward, M. J., Nichols, D., Zdraveva, O., Whitfield, P., and Johns, T., 2008, A decade of tomography: Geophysics, **73**, no. 5, VE5–VE11.